JOURNAL OF GEOPHYSICAL RESEARCH, VOL. 102, NO. D22, PAGES 25,907–25,913, NOVEMBER 27, 1997

# A hotspot function in a simple bidirectional reflectance model for satellite applications

J. M. Chen and J. Cihlar

Applications Division, Canada Centre for Remote Sensing, Ottawa

**Abstract.** The model presented here is an improvement over the semiempirical model of *Roujean et al.* [1992] for estimating the bidirectional reflectance from vegetation. Roujean's model has been considered for global applications because of its simplicity and the underlying physics. However, the model does not adequately describe the hotspot near the Sun's illumination direction. In this paper, a hotspot kernel based on a canopy gap size distribution theory developed by *Chen and Leblanc* [1997] is used to modify Roujean's model. The modified model requires two additional coefficients for controlling the hotspot magnitude and width, respectively. It is found that the hotspot magnitude coefficient is only weakly dependent on cover type and can be treated as a constant at a given geographical location. The hotspot width parameter is determined by the ratio of the characteristic foliage clump size and canopy height. The ratio varies in a small range across different cover types because the foliage clump size and canopy height are usually correlated. For example, the ratio of leaf size to crop height is similar to the ratio of crown size to tree height. Because of the small variabilities of these parameters, the modified model can be a substantial improvement over the original model by just using best estimates for the parameters. With this hotspot adjustment the simple form of the semiempirical model is preserved for remote sensing applications without additional input requirements. The performance of the modified model is shown using data from the advanced very high resolution radiometers (AVHRR). The results show that the patterns of reflectance distribution with the view angle are similar among all cover types investigated, suggesting that one simple model may be sufficient for global applications. The modified model based on simplified physics with four adjustable coefficients may be adequate for this purpose. The model can be further improved to consider the noncircular hotspot shape. Formulae for this purpose are suggested.

## 1. Introduction

Many optical satellites observe the Earth's surface at various angles relative to the surface and the Sun. Since the distributions of reflected solar radiance from vegetated and nonvegetated surfaces are not uniform with the illumination and observation angles, it is often necessary to remove the angular effects in spaceborne and airborne images before the derivation of the surface information, or to use the angular information to detect the surface features. Bidirectional reflectance distribution functions (BRDF) have been used for these purposes. Although numerous sophisticated models based on radiative transfer in plant canopies have been developed [see *Myneni and Ross*, 1991], simple BRDFs are often preferred in image processing [*Walthall et al.*, 1985; *Deering et al.*, 1990; *Dickinson et al.*, 1990; *Jacquemoud et al.*, 1992; *Roujean et al.*, 1992; *Rahman et al.*, 1994; *Wu et al.*, 1995]. *Wanner et al.* [1995] simplified several models into kernels for global applications of the forthcoming moderate-resolution imaging spectrometer (MODIS) [*Salomonson*, 1988].

The physically based simple BRDF model by *Roujean et al.* [1992] is found to perform reasonably well at high latitudes [*Li et al.*, 1996]. In the present study, we found that the model performance deteriorates where the hotspot effect is more pronounced, e.g., for AVHRR data at midlatitudes. This paper presents a modified model which includes a hotspot function while preserving the simplicity of the model. The objective of this study is to derive and validate a simple generic BRDF model for satellite applications.



Paper number 97JD02010.
0148-0227/97/97JD-02010$09.00

## 2. Theory

### 2.1. Evaluation of Roujean's model

In Roujean's model the reflectance from a plant canopy is separated into two parts: geometric and volume scattering. Geometric scattering occurs because of large three-dimensional structures in plant canopies such as tree crowns and crop rows. Volume scattering is caused by foliage elements inside these structures. In the model, simple equations are derived for these two components. The geometrical reflectance ($\rho_{geom}$) is given by

$$\rho_{geom} = \rho_0 \left[ 1 + \frac{hl}{S} f_1(\theta_s, \theta_v, \phi) \right], \quad (1)$$

where $\rho_0$ is the background reflectance; $h$, $l$, and $S$ are the height, length, and the total surface area of the geometrical objects, respectively; $\theta_s$ is the solar zenith angle; and $\theta_v$ is the view zenith angle; $\phi$ is the difference in the azimuthal angle between the Sun and the sensor. The function $f_1$ is defined as

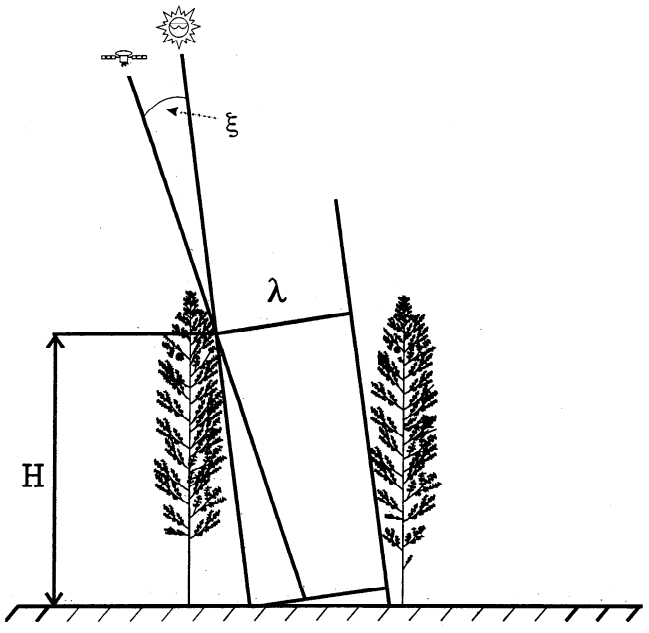


**Figure 1.** An example of the correlation between the illumination and the observation processes: the sunlight and the view line fall into the same canopy gap between trees, where $H$ is the effective canopy height; $\lambda$ is the gap size projected to the Sun's direction; and $\xi$ is the difference in the angle between the Sun and the observer.

$$f_1(\theta_s, \theta_v, \phi) = \frac{1}{2\pi}[(\pi - \phi)\cos\phi + \sin\phi]\tan\theta_s \tan\theta_v - \frac{1}{\pi} \cdot (\tan\theta_s + \tan\theta_v + \sqrt{\tan^2\theta_s + \tan^2\theta_v - 2\tan\theta_s\tan\theta_v\cos\phi}) \quad (2)$$

The volume-scattering reflectance ($\rho_{vol}$) is defined by

$$\rho_{vol} = r[\tfrac{1}{3} + f_2(\theta_s, \theta_v, \phi)](1 - e^{-bF}) + \rho_0 e^{-bF} \quad (3)$$

where $r$ is leaf reflectance, $F$ is leaf area index, $b$ is a constant, and

$$f_2(\theta_s, \theta_v, \phi) = \frac{4}{3\pi}\frac{1}{\cos\theta_s + \cos\theta_v} \cdot \left[\left(\frac{\pi}{2} - \xi\right)\cos\xi + \sin\xi\right] - \frac{1}{3} \quad (4)$$

In (4), $\xi$ is the angle between the observer and the Sun relative to the target, defined as

$$\cos\xi = \cos\theta_s\cos\theta_v + \sin\theta_s\sin\theta_v\cos\phi. \quad (5)$$

The reflectance ($\rho$) of a plant canopy is considered to be the combination of the geometrical and volume-scattering terms; that is,

$$\rho(\theta_s, \theta_v, \phi) = \alpha\rho_{geom} + (1 - \alpha)\rho_{vol} \quad (6)$$

where $\alpha$ is a parameter defining the relative importance of these two components depending on canopy structure and is to be determined empirically.

In the derivation of $\rho_{geom}$ it is assumed that the large structures do not overlap in either illumination or view directions; $\rho_{geom}$ is thus determined by the probability of observing the sunlit side of the individual structures. In the derivation of $\rho_{vol}$ it is assumed that leaves are randomly distributed inside the structures, and a general leaf-scattering phase function is used. In $f_2$ the expressions involving $\xi$ define the shape of the scattering phase function derived by *Ross* [1981] after setting the leaf reflectance to be the same as the leaf transmittance.

In both $\rho_{geom}$ and $\rho_{vol}$, some of the processes contributing to the hotspot have been included; $f_1$ shows the largest probability of observing the sunlit side of the structures when the azimuthal angles of the Sun and observer are the same, corresponding to the fact that the hotspot exists on the sunlit side. The scattering phase function in $f_2$ produces the largest scattering coefficient in the direction of the Sun and hence also contributes to the hotspot. However, these functions only produce a weak hotspot. Since no overlapping of the structures is assumed in the derivation of $f_1$, the modeled reflectances increase continuously with view zenith angle on the sunlit side in the principal solar plane, and in many cases no hotspot can be generated with the model. This model deficiency is apparent in some of the examples in Figures 7 and 8 of *Roujean et al.* [1992] and in results of *Wu et al.* [1995]. This problem is theoretically remedied in the following section.

### 2.2. Modified Model

Roujean's model does not include the major cause for the observed hotspot: the correlation between illumination and observation processes [Kuusk, 1991 [*Myneni and Ross*, 1991]; *Qin and Jupp*, 1993; *Jupp and Strahler*, 1991]. When an observation is made at the same angle as the Sun's illumination, the observer either sees the sunlit foliage or the sunlit background, while all shaded foliage and shaded background are hidden from the view. As the observer moves away from the Sun, more and more of the shaded foliage and the shaded background are exposed to the view. These observation and illumination processes are correlated as long as the view line falls into the same gap as the solar beam; that is, the observer sees the sunlit area through the same gap as the Sun (Figure 1). The correlation ceases as the angle between the Sun and the observer increases to a limit at which these two processes become independent of each other. In this case, the probability of observing a sunlit patch can be taken as the product of two probabilities: one for solar beam illumination and the other for the view line penetration. The angular range in which these two processes remain correlated depends on the canopy gap size, which is the physical dimension of gaps rather than the usual gap fraction or frequency (for the same canopy gap fraction there can be different gap size distributions). *Chen and Leblanc* [1997] recently derived the following theoretical expression to account for this effect based on a canopy gap size distribution function:

$$F(\xi) = \frac{\int_{\lambda_{min}}^{\infty}\left[1 - \frac{\xi}{\tan^{-1}(\lambda/H_\theta)}\right]N(\lambda)\,d\lambda}{\int_{\lambda_{min}}^{\infty}N(\lambda)\,d\lambda} \quad (7)$$

where $F(\xi)$ is a hotspot function, being unity when $\xi = 0$ and zero when $\xi$ exceeds the largest $\tan^{-1}(\lambda/H_\theta)$ value possible. $H_\theta$ is the gap depth in the direction of $\theta_s$. $\lambda_{min}$ is the smallest gap to be included in the integration and depends on the value of $\xi$. $N(\lambda)$ is the number density for canopy gaps of size $\lambda$. It is defined by

$$N(\lambda) = \frac{L_p}{W_p} e^{-L_p(1+\lambda/W_p)} \quad (8)$$

where $L_p$ is the projected area index of the objects responsible for the canopy gaps, and $W_p$ is the characteristic dimension of the objects. In forest stands, the objects causing a large portion of the observed gaps are tree crowns. For the estimation of the hotspot on the ground in forest stands, $L_p$ and $W_p$ can be calculated on the basis of the tree crown area projected on the ground surface (see detailed definitions by *Chen and Leblanc* [1997]). On the tree crowns, gaps between leaves (or shoots in the case of conifer species) also contribute to the hotspot, and the contribution can also be described using a separate $F(\xi)$ function with $L_p$ and $W_p$ defined on the basis of the mean projected leaf (shoot) area on a plane perpendicular to the solar beam. The hotspot kernels for the ground and the crown, denoted by $F_g$ and $F_c$, respectively, can then be used to improve the Roujean's model (equation (6)) in the following manner:

$$\rho(\theta_s, \theta_v, \phi) = \alpha\rho_{\text{geom}}(1 + F_g) + (1 - \alpha)\rho_{\text{vol}}(1 + F_c) \quad (9)$$

The term $(1 + F_g)$ is multiplied with the geometrical reflectance because the ground hotspot component is largely caused by the geometry and the distribution of the tree crowns. $F_g$ enhances the reflectance near the Sun's direction and gradually reduces to zero as the angle between the Sun and the observer increases. Using this hotspot term in the equation also avoids the assumption of nonoverlapping between tree crowns (isolated foliage structures) made in the original Roujean's model and broadens the applicability of the model. Similarly, the term $(1 + F_c)$ also corrects for the problem in the original volume-scattering calculation which does not take into account for the probability of seeing the shaded foliage on the sunlit side of the crown. We believe that by the inclusion of these two hotspot terms, the physics of this semiempirical equation is reasonably complete, and it can handle a wide range of angular reflectance distributions caused by different cover types and densities.

*Chen and Leblanc* [1997] showed that the hotspot kernels for the ground and crown components have very similar shapes because the gap size ($\lambda$) is scaled by the gap depth ($H_\theta$). For the ground component the average gap depth is $H/\cos\theta_s$, where $H$ is the midheight of the canopy at which leaf area density is the largest (shown as the effective canopy height in Figure 1). For the crown component the average gap depth is taken as the mean distance between two layers of leaves in the crown and is related to the leaf area density in the crown. For most cases the ratios of $W_p$ to $H$ for the these two components are similar, and these two kernels can be combined into one for simplicity of model applications. Equation (10) can then be reduced to

$$\rho(\theta_s, \theta_v, \phi) = [\alpha\rho_{\text{geom}} + (1 - \alpha)\rho_{\text{vol}}](1 + F) \quad (10)$$

where $F$ is a hotspot function representing the hotspot magnitude due to both the ground and the crown reflectance enhancement around the Sun.

The exact expression of the hotspot kernel (equation (7)) involves the integration with respect to the gap size number density and is not easily used in image processing. Its calculation also requires input of canopy height and density (tree density in the case of forested surfaces). For many satellite application purposes, (7) can be substituted by the following simpler form chosen for its ability to approximate the hotspot curve shape produced by (7):

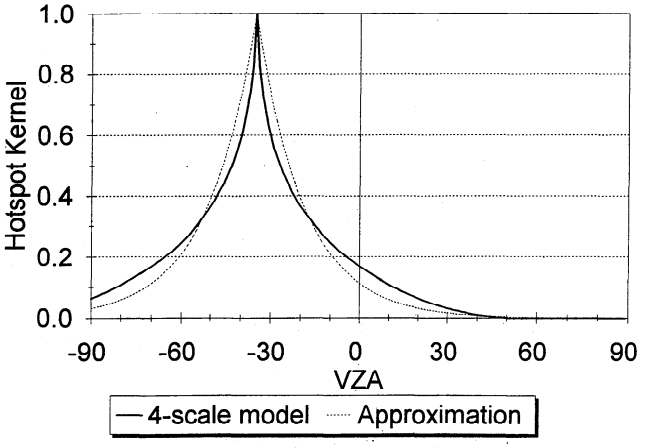


**Figure 2.** Hotspot kernels calculated by using a complete equation (equation (7)) and an approximated equation (equation (11)).

$$F(\xi) = C_1 e^{-(\xi/\pi)C_2} \quad (11)$$

where $C_1$ determines the magnitude of the hotspot, and $C_2$ controls the width of the hotspot. $C_1$, by the physical meaning, is linearly related to the difference between the reflectances of the foliage and the background at the wavelengths of interest. $C_2$ is proportional to the ratio of the canopy height to the size of the predominant canopy structures such as tree crowns, and the proportionality is controlled by the density of the structures such as stems/ha, which is linearly related to the projected crown area index $L_p$. More precisely, $C_2$ is proportional to $L_pH_\theta/W_p$. Figure 2 shows the complete and approximate calculations of $F$ using (7) and (11) for the crown or the ground components with parameters of $L_p = 3$, $H_\theta = 10$ m, and $W_p = 2$ m for the ground component, or $L_p = 3$, $H_\theta = 0.2$ m, and $W_p = 0.04$ m for the crown component. The empirical coefficients used for (11) are $C_1 = 1.0$ and $C_2 = 11.0$. The simplified (11) approximates closely (7) for the complete calculation of the hotspot. It is also seen from the parameters used that the hotspot distributions for the ground and crown components are similar, justifying the use of only one kernel in the semiempirical equation.

After rearranging (11) and factoring out the sum of non-functional terms as a constant, which is treated as the reflectance at nadir by *Wu et al.* [1995], (10) is rewritten as

$$\rho(\theta_s, \theta_v, \phi) = \rho(0, 0, \phi)(1 + a_1 f_1(\theta_s, \theta_v, \phi) + a_2 f_2(\theta_s, \theta_v, \phi)(1 + C_1 e^{-(\xi/\pi)C_2}) \quad (12)$$

Compared with the Roujean's model (equation (6)), (12) has two additional constants $C_1$ and $C_2$. Although these constants increase the complexity somewhat, they improve the flexibility of the model to simulate a wide range of the BRDF shapes based on physical principles.

## 3. Application of the Modified Model

As this study stems from the need to improve our methodology for BRDF corrections in processing AVHRR composite images, the usefulness of the modified model is first tested by using AVHRR data. Figure 3 shows the improvements of the modified model over the original model for four dominant cover types in North America. This set of data was originally

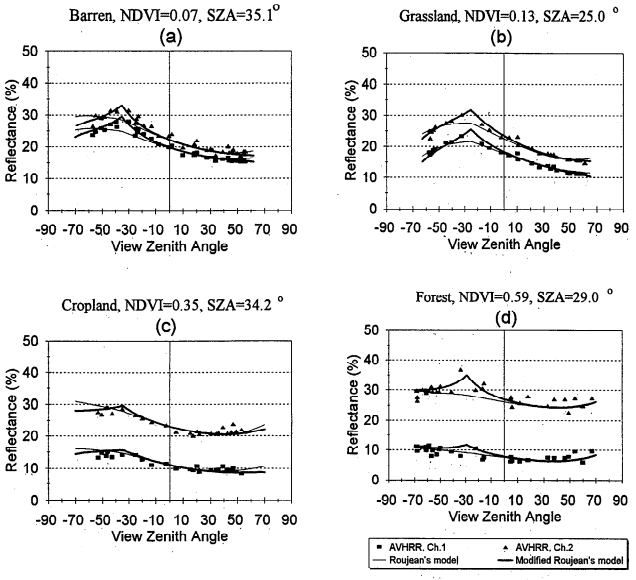


**Figure 3.** Advanced very high resolution radiometer (AVHRR) measurements near the principal solar plane and their simulations using the original and modified Roujean's models for four cover types at midlatitudes.

shown by *Wu et al.* [1995] and was obtained from NOAA 11 AVHRR data acquired in three growing seasons (April–October 1990–1992) over the conterminous United States and southern Canada [*Hood*, 1993]. Careful geometrical and radiometric calibrations and cloud screening were performed on the data set (see details by *Wu et al.* [1995]). The data were stratified according to solar zenith angle and normalized difference vegetation index (NDVI) to reduce the noise in the angular reflectance distribution, and most observations were made within a narrow range (±30°) from the principal solar plane (PSP). For all four cover types, the variation in reflectance with view zenith angle in the PSP is very pronounced, and a hotspot at the solar zenith angle is clearly discernible in each case. The original Roujean's model is able to simulate the observations reasonably well and also shows some hotspot effect, especially for the case of grassland. This small hotspot in the model is mostly obtained in the geometrical term ($f_1$) which considers the probability of observing the sunlit side of unobstructed objects. This term not only defines the magnitude of the hotspot but also its slope from the backscattering to the forward scattering side. It is not possible within the model flexibility to enhance the hotspot without changing the slope. For the cases (cropland and forest) where the general slope from backscattering to the forword scattering side is small, no obvious hotspots can be produced using the original model. The volume-scattering term ($f_2$) enables the adjustment of the upward curvature of the curve (the bowl shape) and does not contribute significantly to the hotspot. In Figure 3, considerable improvements of the modified model over the original model are evident in the simulation of data for barren and grassland, with the root-mean-square-error (RMSE) reduced from 0.0099 to 0.0058 for barren and from 0.0061 to 0.0059 for grassland in channel 1, and from 0.0128 to 0.0091 and from 0.0079 to 0.0052 in channel 2, respectively. For cropland and forest the improvements in the RMSE values are much smaller because of the smaller hotspot amplitudes. With the inclusion of the specific hotspot term, the model captures the observed reflectance peak near solar zenith angle very well. The two coefficients in this term have the critical functions of defining the magnitude ($C_1$) and width ($C_2$) of the peak. With this modification the model now has all the necessary flexibility to simulate an observed BRDF: $a_1$ for the general backward to forward scattering slope, $a_2$ for the bowl shape, $C_1$ for the hotspot magnitude, and $C_2$ for the hotspot width. We emphasize that all the terms in the original and modified Roujean's models are based on physics rather than curve-fitting mathematics, although the physics has to be much simplified for remote sensing applications.

In Table 1 the $a_1$ and $a_2$ values for Roujean's model are similar to those recommended by *Wu et al.* [1995] for the various data sets with different NDVI values but adjusted for these data sets. The $a_1$ and $a_2$ values for the modified model are further adjusted to accommodate the inclusion of the hotspot function. The adjustments are made to achieve the minimum RMSE values. It is noted that $C_1$ and $C_2$ vary in a small range among the cover types. Because of the noise in the data, the model simulation through curve fitting is not very sensitive to $C_2$, and a value of 10 is a good approximation for all cover types at midlatitudes. The distribution patterns are remarkably similar among all cover types within the range of observation angles, suggesting that BRDF of different underlying surfaces

**Table 1.** Coefficients Used in Figure 2 in Roujean's Model (RM) and Modified Roujean's Model (MRM)

| | | Channel 1 (Visible) | | | | Channel 2 (Near Infrared) | | | |
|---|---|---|---|---|---|---|---|---|---|
| Cover Type | Model | $a_1$ | $a_2$ | $C_1$ | $C_2$ | $a_1$ | $a_2$ | $C_1$ | $C_2$ |
| Cropland | MRM | 0.30 | 2.0 | 0.30 | 6.67 | .10 | 1.4 | 0.40 | 8.33 |
| | RM | 0.20 | 2.50 | ··· | ··· | 0.10 | 2.00 | ··· | ··· |
| | RM-Wu | 0 | 2.1 | ··· | ··· | 0 | 1.44 | ··· | ··· |
| Forest | MRM | 0 | 3.0 | 0.80 | 12.50 | 0.05 | 1.20 | 0.65 | 12.50 |
| | RM | 0 | 3.0 | ··· | ··· | 0.05 | 1.2 | ··· | ··· |
| | RM-Wu | 0 | 3.04 | ··· | ··· | 0 | 1.96 | ··· | ··· |
| Barren | MRM | 0.30 | 1.3 | 0.65 | 11.11 | 0.30 | 1.4 | 0.60 | 12.50 |
| | RM | 0.25 | 1.8 | ··· | ··· | 0.25 | 2.0 | ··· | ··· |
| | RM-Wu | 0.21 | 1.63 | ··· | ··· | 0.21 | 1.52 | ··· | ··· |
| Grassland | MRM | 0.63 | 2.0 | 0.6 | 10 | 0.50 | 2.5 | 0.50 | 8.33 |
| | RM | 0.55 | 2.5 | ··· | ··· | 0.45 | 3.0 | ··· | ··· |
| | RM-Wu | 0.30 | 1.14 | ··· | ··· | 0.4 | 1.20 | ··· | ··· |

The coefficients in RM used by *Wu et al.* [1995] (RM-Wu) are also given for comparison.

can be simulated effectively using one basic model by adjusting its coefficients.

The modified model has been used in our operational processing of AVHRR composite images of Canada acquired in 1993 and resampled to 1 km resolution. Ten-day cloud-free composites were produced by using the geocoding and compositing system (GEOCOMP) [*Robertson et al.*, 1992] with the maximum-NDVI pixel selection criterion to screen the clouds. The GEOCOMP produces 10 channel outputs, which include radiance for bands 1–5, NDVI, view zenith angle, solar zenith angle, Sun-sensor azimuthal angle difference, and the date of acquiring the selected pixel. The radiance in bands 1 and 2 was converted into top-of-atmosphere reflectance in subsequent processing using band-specific solar irradiance above the atmosphere [*Cihlar et al.*, 1997a]. Figure 4 shows improvements in BRDF corrections made using the modified model for coniferous forests in central Canada (Saskatchewan and Manitoba) of a 1200 km × 1200 km area [*Cihlar et al.*, 1997b]. Five thousand data points are randomly selected from approximately 500,000 data points for the conifer cover type in the image. The impact of the atmospheric correction is more significant in channel 1 than in channel 2 because of the strong Rayleigh scattering at the visible wavelengths. The remaining large angular variations in both channels after the atmospheric corrections were fitted using Roujean's model and removed by normalizing the individual reflectance value to that at $\theta_v = 0°$ and $\theta_s = 45°$. The improvements made by Roujean's model are very pronounced in both channels (third panels in Figure 4), as evidenced in the large reductions in the standard deviation in reflectance. However, the resultant reflectance distributions in both channels have a peak of considerable size at the view zenith angle of about 52° on the backscattering side where the sensor and solar angles coincide. When the same model fitting and normalizing approaches are applied to the atmospherically corrected data using the modified model, the angular dependence is further reduced and so is the standard deviation, confirming the improvements of the modified model over the original model. In using the modified Roujean model, the original coefficients for the geometrical and volume-scattering terms found by *Li et al.* [1996] were modified because without considering the hotspot, the model could not simulate the wavy features and has to chose values which represent a large angle range around the hotspot. With the use of the additional hotspot function, the modified model has enough flexibility to handle the pronounced hotspot as well as the curvature in the forward scattering direction. The coefficients used for channel 1 are −0.3, 1.5, 1.6, and 6.0 for $a_1$, $a_2$, $C_1$, and $C_2$, respectively. For channel 2 the corresponding values are −0.6, 2.5, 2.0, and 4.0. The simulation is more sensitive to $a_1$ and $a_2$ than to $C_1$ and $C_2$. All these values are considerably different from those listed in Table 1, suggesting that these coefficients depend not only on the cover type but also on latitude. The values of $C_1$ are larger than those in Table 1 because the background signal is stronger from open boreal forests than from dense forests at midlatitudes. The values of $C_2$ are smaller because of the shorter trees, less leaf area, and denser and smaller tree crowns at height latitudes. $C_2$ for channel 2 is found to be smaller than that for channel 1 in the simulation. Since smaller $C_2$ values produce broader hotspots, this suggests a larger influence of multiple scattering in near infrared than in visible wave band. Similar improvements using the modified model are also found for other cover types. The latitudes at which the hotspot effects are most pronounced depend on the solar declination and the time of local overpasses of the AVHRR sensor. The cases presented in Figure 4 have strong hotspot effects because of the shift in the overpass time of the NOAA 11 AVHRR sensor toward late afternoon. For the new NOAA 14 AVHRR sensor and other Earth observation satellite sensors with local overpass time near noon it is expected that the ability of making hotspot corrections is more important at low and midlatitudes than at high latitudes.

## 4. Discussion

Several simple models have been produced for BRDF corrections in remote sensing imagery [*Shibayama and Wiegand*, 1985; *Walthall et al.*, 1985; *Deering et al.*, 1990]. Compared with Roujean's model, these models are simpler and have the basic functionalities to simulate the bowl shape and the slope of the reflectances from the backward to forward scattering direction. However, none of these empirical models has the ability to simulate the curvature around the hotspot. *Hautecoeur and Leroy* [1996] compared these models with Roujean's model and with another more sophisticated curve-fitting model based on spherical harmonics. They found that while the spherical harmonic model offers more flexibility than the Roujean's model in data simulation, it is also internally unstable when the data are not complete because of its purely mathematical nature. Roujean's model outperformed other simpler empirical models and also appeared to be more stable in the model inversion than the spherical harmonic model. Roujean's model not only has the necessary simplicity for remote sensing applications but more importantly, it includes the basic physics. Although the radiative transfer physics is very much simplified in Roujean's model, it has more generality than the empirical models constructed for the need of curve or surface fitting. We believe that the use of the hotspot terms in Roujean's model has increased its generality and made it more flexible for various cover types and geographic areas.

The underlying assumption made in using one coefficient controlling the hotspot width is that the hotspot has a circular shape in the cylindrical coordinate. In many cases, elliptical hotspot shapes are found [*Li and Strahler*, 1992; *Bicheron et al.*, 1997]. In the four-scale model [*Chen and Leblanc*, 1997], this hotspot shape can be simulated by considering the dependence of the projected tree crown width on the azimuthal angle difference between the Sun and the sensor. The modified model can also be improved in this respect by allowing the hotspot width to change with the azimuth angle in the following way:

$$\rho(\theta_s, \theta_v, \phi) = \rho(0, 0, \phi)(1 + a_1 f_1(\theta_s, \theta_v, \phi)) + a_2 f_2(\theta_s, \theta_v, \phi)(1 + C_1 e^{-(\xi/\pi)C_2(\xi, \phi)}) \quad (13)$$

where

$$C_2(\xi, \phi) = \frac{C_{2a}C_{2b}}{\sqrt{C_{2a}^2 \sin^2(\alpha(\xi, \phi)) + C_{2b}^2 \cos^2(\alpha(\xi, \phi))}}. \quad (14)$$

In (14), $C_{2a}$ and $C_{2b}$ are constants controlling the hotspot width along and perpendicular to the principal solar plane, respectively, and $\alpha$ is the angle between the principal solar plane and the line joining the hotspot and the point of interest (Figure 5). From the trigonometry, $\alpha$ can be defined as

$$\alpha(\xi, \phi) = \pi - \phi - \sin^{-1}\left(\frac{\sin\theta_s}{\sin\xi}\sin\phi\right) \quad (15)$$

With these formulae it is fairly straightforward to simulate the

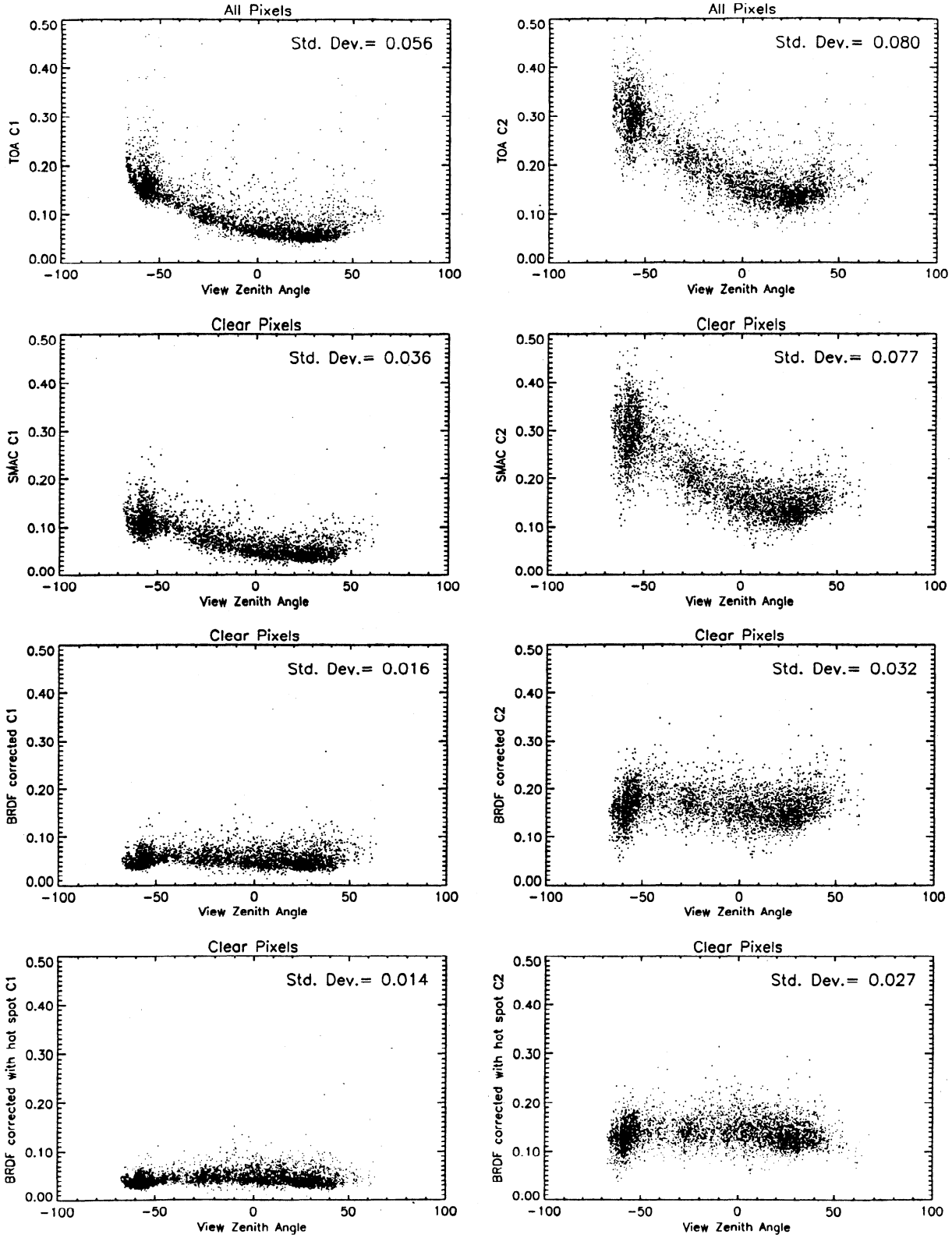


**Figure 4.** Improvements achieved by original and modified Roujean's model in AVHRR image processing for conifer forests in central Canada. It shows AVHRR channel 1 data on the left-hand side and channel 2 on the right-hand side. From the top to bottom are reflectance values (1) at the top of the atmosphere, (2) after atmospheric corrections using SMAC (simplified model for atmospheric corrections) [*Rahman et al.*, 1994], (3) after bidirectional reflectance distribution function (BRDF) corrections using Roujean's model, and (4) after BRDF corrections using the modified model. The "Std. Dev." shown in each plot is the standard deviation of the reflectance (on the vertical axis). At the latitudinal range from 50° to 60° the solar zenith angle across the swath from the view zenith angle of −69° to +69° changes approximately linearly from 60° to 40° [*Li et al.*, 1996], and therefore the hotspot, where the view and solar angles are the same, should appear at a zenith angle of about 52.4°. AVHRR measurements at these latitudes were made very close to the principal solar plane; that is the sensor-Sun azimuthal angle difference is close to zero in the backscattering direction and 180° in the forward scattering direction.

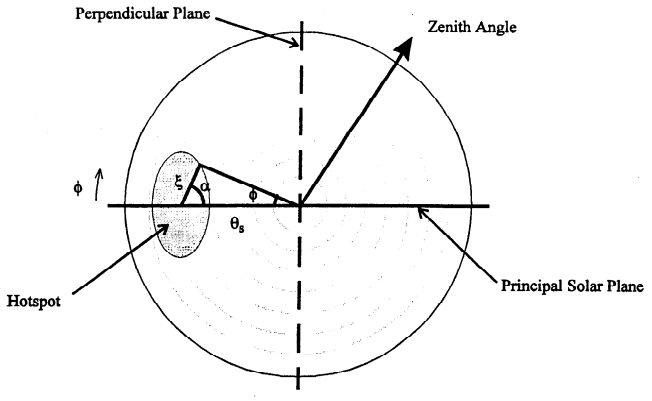


**Figure 5.** Schematic description of a noncircular hotspot in the cylindrical coordinate system, where $\theta_s$ is the solar zenith angle; $\phi$ is the azimuthal angle difference between the Sun and the observer; $\xi$ is the angle between the Sun and the observer; and $\alpha$ is the azimuthal angle around the hotspot defined by equation (15).

elliptical hotspot shape by providing the appropriate $C_{2a}$ and $C_{2b}$ values.

## 5. Conclusions

On the basis of the physics of radiation interaction with plant canopies, Roujean's model is modified to explicitly describe the hotspot. The hotspot kernel derived by *Chen and Leblanc* [1997] on the basis of canopy gap size distribution is simplified for remote sensing applications in this paper. This modification overcomes problems in original Roujean's model due to the assumption of nonoverlapping in illumination and observation directions between geometrical structures such as tree crowns. This modification also takes into account for the mutual shadowing effects between layers of leaves which was not considered in original Roujean's model. This modified model contains four adjustable coefficients for controlling the shape of the reflectance distribution with view angle, the slope of the slant from backward to forward scattering direction, the hotspot width, and hotspot magnitude. These four coefficients may be the minimum required for BRDF simulations. The improvement made by this modification is demonstrated in the processing of AVHRR data at middle and high latitudes. An important feature of this modified model is that each component is based on radiation physics rather than on empirical curve or surface fitting techniques so that it provides generality needed for applications for various cover types. Such a physically based model can also be further expanded for the needs to simulate the noncircular hotspot shape. Formulae for this purpose are suggested.

**Acknowledgments.** We thank A. Wu and Z. Li for the provision of data in Figure 3 and F. Huang and S. Leblanc for technical assistance.

## References

Bicheron, P., M. Leroy, F. M. Breon, and O. Hautecoeur, Anhanced discrimination of boreal forest covers with directional reflectances from the airborne POLDER instrument, *J. Geophys. Res.*, in press, 1997.

Chen, J. M., and S. Leblanc, A four-scale bidirectional reflectance model based on canopy architecture, *IEEE Trans. Geosci. Remote Sens.*, in press, 1997.

Cihlar, J., H. Ly, Z. Li, J. M. Chen, H. Pokrant, and F. Huang, Multitemporal, multichannel AVHRR data sets for land biosphere studies—Artifacts and corrections, *Remote Sens. Environ.*, *60*, 35–57, 1997a.

Cihlar, J., J. M. Chen, and Z. Li, Seasonal AVHRR multichannel data sets and products for studies of surface-atmosphere interactions, *J. Geophys. Res.*, in press, 1997b.

Deering, D. W., T. F. Eck, and J. Otterman, Bidirectional reflectance model of the Earth's surfaces and their three-parameter soil characterization, *Agric. For. Meteorol.*, *52*, 71–93, 1990.

Dickinson, R. E., B. Pinty, and M. M. Verstaete, Relating surface albedo in GCMs to remotely sensed data, *Agric. For. Meteorol.*, *32*, 109–131, 1990.

Hautecoeur, O., and M. Leory, Intercomparison of several BRDF models for the compositing of spaceborne POLDER data over land surfaces, *Proc. Int. Geosci. Remote Sens. Symp.*, *1*, 204–208, 1996.

Hood, J. J., Advanced Very High Resolution Radiometer validation data set, in *25th International Symposium on Remote Sensing and Global Environmental Change*, *ERIM Joanneum Res./CIESIN, Graz, Austria*, 1993.

Jacquemoud, S., F. Baret, and J. F. Hanocq, Modeling spectral and bidirectional soil reflectance, *Remote Sens. Environ.*, *41*, 123–132, 1992.

Jupp, D. L. B., and A. H. Strahler, A hot-spot model for leaf canopies, *Remote Sens. Environ.*, *38*, 193–210, 1991.

Li, X., and A. H. Strahler, Geometric optical bidirectional reflectance modeling of the discrete crown vegetation canopy: Effect of crown shape and mutual shadowing, *IEEE Trans. Geosci. Remote Sens.*, *24*, 906–919, 1992.

Li, Z., J. Cihlar, X. Zheng, L. Moreau, and H. Ly, The bidirectional effects of AVHRR measurements over boreal regions, *IEEE Trans. Geosci. Remote Sens.*, *34*, 1308–1322, 1996.

Myneni, R. B., and J. Ross, *Photon-Vegetation Interactions*, Springer-Verlag, New York, 1991.

Qin, W., and D. L. B. Jupp, An analytical and computationally efficient reflectance model for leaf canopies, *Agric. Meteorol.*, *66*, 31–64, 1993.

Rahman, H., and G. Dedieu, SMAC: A simplified method for atmospheric correction of satellite measurements in the solar spectrum, *Int. J. Remote Sens.*, *15*, 123–143, 1994.

Rahman, H., B. Pinty, and M. M. Verstraete, A coupled surface-atmosphere reflectance (CSAR) model, part 2: A semiempirical surface model usable with NOAA/AVHRR data, *J. Geophys. Res.*, *98*, 207–20801, 1994.

Robertson, B., A. Erickson, J. Friedel, B. Guindon, T. Fisher, R. Brown, P. Teillet, M. D'Iorio, J. Cihlar, and A. Sancz, GEOCOMP, a NOAA AVHRR geocoding and compositing system, in *Proceedings of the ISPRS Conference*, pp. 223–228, Int. Soc. for Photogramm. and Remote Sens., Washington, D. C., 1992.

Ross, J., *The Radiation Regime and Architecture of Plant Stands*, Dr. W. Junk, New York, 1981.

Roujean, J.-L., M. J. Leroy, and P.-Y. Deschamps, A bidirectional reflectance model of the Earth's surface for the correction of remote sensing data, *J. Geophys. Res.*, *97*, 20,455–20,468, 1992.

Salomonson, V. V., The Moderate Resolution Imaging Spectrometer (MODIS), *IEEE Geosci. Remote Sens. Newslet.*, *12*(3), 11–15, 1988.

Shibayama, M., and C. J. Wiegand, View azimuth and zenith, and solar angle effects on wheat canopy reflectances, *Remote Sens. Environ.*, *18*, 91–103, 1985.

Walthall, C. L., J. M. Norman, J. M. Welles, G. Campbell, and B. L. Blad, Simple equation to approximate the bidirectional reflectance from vegetation canopies and bare soil surfaces, *Appl. Opt.*, *24*, 383–387, 1985.

Wanner, W., X. Li, and A. H. Strahler, On the derivation of kernals for kernal-driven models of bidirectional reflectance, *J. Geophys. Res.*, *100*, 21,077–21,090, 1995.

Wu, A., Z. Li, and J. Cihlar, Effects of land cover type and greenness on advanced very high resolution radiometer bidirectional reflectances: Analysis and removal, *J. Geophys. Res.*, *100*, 9179–9191, 1995.

J. M. Chen and J. Cihlar, Applications Division, Canada Centre for Remote Sensing, 588 Booth Street, Ottawa, Ontario, Canada K1A 0Y7. (e-mail: jing.chen@ccrs.nrcan.gc.ca)

(Received December 12, 1996; revised July 3, 1997; accepted July 12, 1997.)